

Article

Synthesis, DFT Study, and In Vitro Evaluation of Antioxidant Properties and Cytotoxic and Cytoprotective Effects of New Hydrazones on SH-SY5Y Neuroblastoma Cell Lines

Diana Tzankova¹, Hristina Kuteva², Emilio Mateev¹ , Denitsa Stefanova², Alime Dzhemadan², Yordan Yordanov² , Alexandrina Mateeva¹, Virginia Tzankova², Magdalena Kondeva-Burdina², Alexander Zlatkov¹  and Maya Georgieva^{1,*}

¹ Department “Pharmaceutical Chemistry”, Faculty of Pharmacy, Medical University-Sofia, 2 Dunav Str., 1000 Sofia, Bulgaria; d.tsankova@pharmfac.mu-sofia.bg (D.T.); e.mateev@pharmfac.mu-sofia.bg (E.M.); a.dineva@pharmfac.mu-sofia.bg (A.M.); azlatkov@pharmfac.mu-sofia.bg (A.Z.)

² Laboratory “Drug metabolism and Drug Toxicity”, Department “Pharmacology, Pharmacotherapy and Toxicology”, Faculty of Pharmacy, Medical University-Sofia, 2 Dunav Str., 1000 Sofia, Bulgaria; hristina.kuteva@abv.bg (H.K.); denitsa.stefanova@pharmfac.mu-sofia.bg (D.S.); yyordanov@pharmfac.mu-sofia.bg (Y.Y.); vtzankova@pharmfac.mu-sofia.bg (V.T.); mkondeva@pharmfac.mu-sofia.bg (M.K.-B.)

* Correspondence: mgeorgieva@pharmfac.mu-sofia.bg

Abstract: A series of ten new hydrazide–hydrazone derivatives bearing a pyrrole ring were synthesized and structurally elucidated through appropriate spectral characteristics. The target hydrazones were assessed for radical scavenging activity through 1,1-diphenyl-2-picrylhydrazyl (DPPH) and 2,2′-azino-bis(3-ethylbenzothiazoline-6-sulphonic acid) (ABTS) tests, with ethyl 5-(4-bromophenyl)-1-(2-(2-(4-hydroxy-3,5-dimethoxybenzylidene)hydrazine-yl)-2-oxoethyl)-2-methyl-1H-pyrrole-3-carboxylate (**7d**) and ethyl 5-(4-bromophenyl)-1-(3-(2-(4-hydroxy-3,5-dimethoxybenzylidene)hydrazine-yl)-3-oxopropyl)-2-methyl-1H-pyrrole-3-carboxylate (**8d**) highlighted as the best radical scavengers from the series. Additional density functional theory (DFT) studies have indicated that the best radical scavenging ligands in the newly synthesized molecules are stable, do not decompose into elements, are less polarizable, and with a hard nature. The energy of the highest occupied molecular orbital (HOMO) revealed that both compounds possess good electron donation capacities. Overall, **7d** and **8d** can readily scavenge free radicals in biological systems via the donation of hydrogen atoms and single electron transfer. The performed in vitro assessment of the compound’s protective activity on the H₂O₂-induced oxidative stress model on human neuroblastoma cell line SH-SY5Y determined **7d** as the most perspective representative with the lowest cellular toxicity and the highest protection.

Keywords: pyrrole; synthesis; DFT; antioxidant; SH-SY5Y; cellular toxicity; cell protection



Citation: Tzankova, D.; Kuteva, H.; Mateev, E.; Stefanova, D.; Dzhemadan, A.; Yordanov, Y.; Mateeva, A.; Tzankova, V.; Kondeva-Burdina, M.; Zlatkov, A.; et al. Synthesis, DFT Study, and In Vitro Evaluation of Antioxidant Properties and Cytotoxic and Cytoprotective Effects of New Hydrazones on SH-SY5Y Neuroblastoma Cell Lines. *Pharmaceuticals* **2023**, *16*, 1198. <https://doi.org/10.3390/ph16091198>

Academic Editor: Valentina Noemi Madia

Received: 29 July 2023

Revised: 17 August 2023

Accepted: 18 August 2023

Published: 23 August 2023



Copyright: © 2023 by the authors. Licensee MDPI, Basel, Switzerland. This article is an open access article distributed under the terms and conditions of the Creative Commons Attribution (CC BY) license (<https://creativecommons.org/licenses/by/4.0/>).

1. Introduction

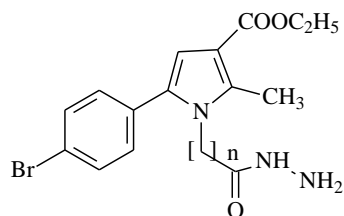
The generation of reactive oxygen species (ROS) leads to oxidative damage to biomolecules, such as cellular proteins, lipids, and DNA, and, as a result, to disruption to normal cellular functions [1]. A gradual decline in cellular antioxidant defense mechanisms due to the generation of ROS during aging leads to increases in oxidative stress. Therefore, aging, various genetic mutations, the influence of the environment, and the associated increase in oxidative stress are a prerequisite for the development of many neurodegenerative diseases, including Parkinson’s disease (PD), Alzheimer’s disease (AD), Huntington’s disease (HD), amyotrophic lateral sclerosis (ALS), and many others [2]. Accordingly, the discovery of novel active substances with antioxidant potential is the basis of many programs for providing effective neuroprotection in the therapy of neurodegenerative diseases [3].

A lot of market drugs containing pyrrole ring show different pharmacological activities, such as antipsychotics [4], antidepressants [5], anticonvulsants [6], anti-inflammatories [7],

and many others. There is increased interest in pyrroles and pyrrole derivatives exhibiting proven antioxidant effects [8,9]. Many heterocyclic hydrazones have shown antioxidant and neuroprotective activity, too [10].

For example, Boulebd et al. [11] successfully synthesized a series of new phenolic hydrazide-hydrazone derivatives and tested them for radical scavenging activity using DPPH and ABTS methods. The effects were compared with the action of ascorbic acid and Trolox, compounds with proven antioxidant activity. It was found that the synthesized new derivatives exhibited antioxidant activity comparable to those of ascorbic acid and Trolox [11]. In another study [12], twelve heterocyclic compounds bearing hydrazone functional groups were evaluated for antioxidant activity using DPPH, ABTS, and DMSO alkaline assays. The results showed that these heterocyclic compounds are potent anti-radical agents [12]. In addition, a preliminary study performed by Tzankova et al. [13] identified the promising radical scavenging potential of pyrrole-based hydrazones, as determined through DPPH and ABTS assays, which pointed our attention toward the synthesis of analogous representatives in an attempt to enrich the variety of molecules.

In the current study, the initial hydrazides were synthesized in our laboratory, as previously explained in detail by Bijev et al. [14] for hydrazone 7 and Georgieva et al. [15] for hydrazone 8, with the general structure presented in Figure 1.



$n = 1$ (7) and $n = 2$ (8)

Figure 1. General structure of the initial pyrrole hydrazides.

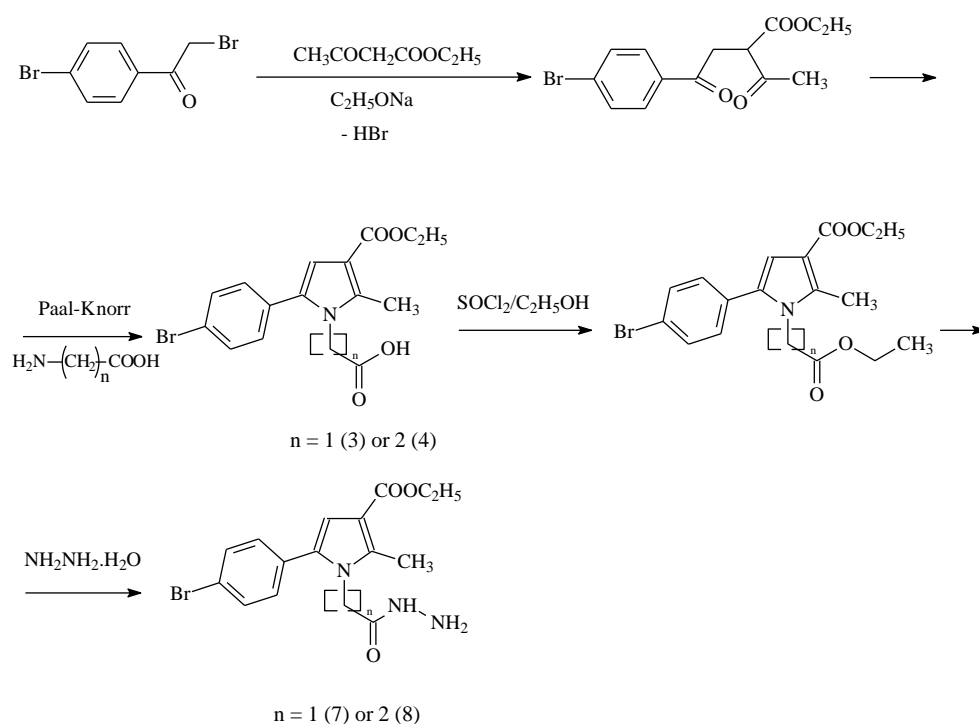
The following study is focused on the synthesis of new hydrazones containing a pyrrole ring system and the evaluation of their *in vitro* safety profile on human neuroblastoma SH-SY5Y cells, radical scavenging activity through 1,1-diphenyl-2-picrylhydrazyl (DPPH) and 2,2'-azino-bis(3-ethylbenzothiazoline-6-sulphonic acid) (ABTS) assays and *in silico* assessment of possible antioxidant mechanisms through DFT calculations. The most promising structures are evaluated for antioxidative protective properties in a H_2O_2 -induced oxidative stress model on SH-SY5Y cells.

2. Results

2.1. Chemistry

2.1.1. Synthesis of the N-pyrrolyl hydrazides 7 (ethyl 5-(4-bromophenyl)-1-(2-hydrazinyl-2-oxoethyl)-2-methyl-1H-pyrrole-3-carboxylate) and 8 (ethyl 5-(4-bromophenyl)-1-(3-hydrazinyl-3-oxopropyl)-2-methyl-1H-pyrrole-3-carboxylate)

The pyrrole ring in the target hydrazone molecules was formed through a Paal-Knorr cyclization reaction based on the C-alkylation of a 1,3-dicarbonyl compound to the corresponding 1,4-dicarbonyl derivative (2), cycled afterward with the corresponding amino acids L-glycine ($n = 1$) and L- β -alanine ($n = 2$) to give the following N-substituted pyrrole carboxylic acids (3 and 4, respectively). An esterification of the obtained acids was conducted, followed by a hydrazinolysis reaction with hydrazine hydrate, to give the target hydrazides (7 and 8, respectively) according to the procedure presented in Scheme 1 and described in detail in [14,15].



Scheme 1. Synthesis of the initial hydrazides **7** and **8** [14,15].

2.1.2. Synthesis of the New N-pyrrolylhydrazide-hydrazone **7a-e** and **8a-e**

The novel series of N-pyrrolylhydrazide-hydrazone derivatives were prepared under microsynthesis scale conditions through condensation reaction from the previously synthesized in our laboratory hydrazides **7** and **8** and the selected carbonyl partners (Figure 2), assuring about 64–86% yield of the purified product. The new compounds were synthesized according to the procedure presented in Scheme 2.

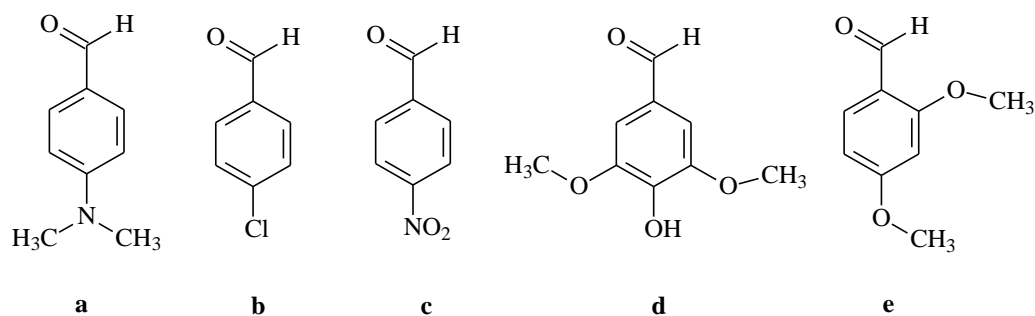
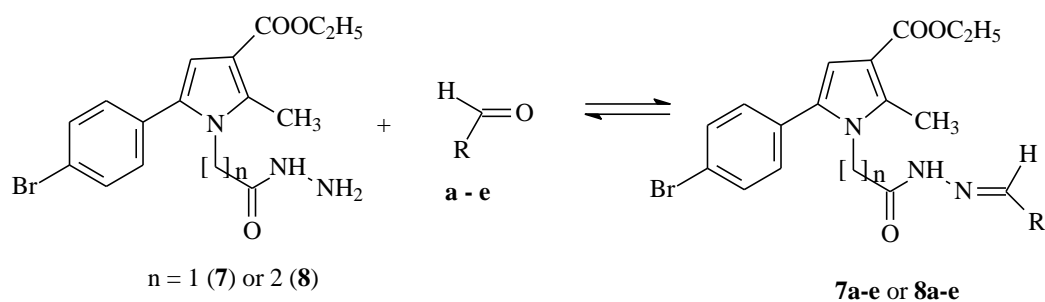


Figure 2. Used aldehydes (**a-e**).



Scheme 2. Synthesis of the new hydrazone compounds.

The reaction conditions were altered, as presented in Table 1, wherein the reflux in glacial acetic acid was selected as the most appropriate. All the new derivatives were obtained according to that presented in the Materials and Methods section procedures.

Table 1. Reaction conditions, reaction times, and yields.

Reaction Media	Reaction Temperature °C	Reaction Time (min)	Yields %
Ethanol	Heating	50–60	46–80
Ethanol + HCl	Room temperature	20–30	56–94
Methanol + conc. HCl	Room temperature	1440	15–56
Ethanol + glacial acetic acid	100 °C	30–50	26–64
Glacial acetic acid	100 °C	20–30	68–84

The synthesized pyrrole hydrazones are stable at room temperature for long periods of time. The structures of the new compounds were elucidated by melting points, TLC characteristics, IR, and ¹H-NMR spectral data, followed by MS data. The results from the spectral analysis confirmed that the new compounds are consistent with the expected structure. The corresponding experimental IR, ¹H-NMR, and LC-MS spectra of the target derivatives are supplied as Supplementary Materials. The purity of the obtained compounds was proven by corresponding elemental analyses.

The IR data determine the presence of new signals at 3245 cm⁻¹ for the valence asymmetric (ν^{as}) vibrations for the amide NH group in the molecule of the new hydrazones and a band at 1666 cm⁻¹ (Amide I) and 1533 cm⁻¹ for deformational (δ) vibrations of the amide NH group (Amide II). In addition, the appearance of a band at around 810 cm⁻¹ determines the presence of *p*-substituted phenyl residue. The ester group (COOC₂H₅) in the third position in the central pyrrole ring is pointed by the appearance of a band at around 1693–1698 cm⁻¹. A confirmation of the structural elucidation may be seen in the relevant ¹H NMR spectra, where the corresponding groups are available at 7.86 ppm for the CH=N group and at 11.38 ppm for the CONH group, respectively. The obtained values from the experimental spectral data are consistent with the theoretical ones.

The corresponding IDs, melting points, TLC characteristics, MS data, and yields are given in Table 2. The respective IR characteristics and ¹H-NMR spectral data are presented in the Materials and Methods section.

Table 2. IDs, melting points, TLC characteristics (Rf), MS data, and yields for the new N-pyrrolyl-hydrazones.

IDs	m.p. °C	Rf	MS Data [M+H] ⁺ (m/z)	Yields %
7a	211.4–213.6	0.38	511.13	84
7b	229.4–231.2	0.33	502.05	78
7c	245.9–247.2	0.33	512.07	76
7d	191.9–194.4	0.29	544.10	68
7e	206.0–207.6	0.40	528.11	72
8a	212.0–213.3	0.35	525.15	86
8b	181.4–184.6	0.31	517.06	74
8c	214.4–217.1	0.33	527.09	82
8d	196.6–197.6	0.28	558.12	64
8e	170.0–171.9	0.34	542.13	74

2.2. Antioxidant Assays

2.2.1. DPPH Radical Scavenging Assay

The 1,1-diphenyl-2-picrylhydrazyl (DPPH) radical scavenging activity of the newly synthesized derivatives was determined at one concentration—1 mg/mL. Trolox was used as a standard. The obtained results are presented in Figure 3.

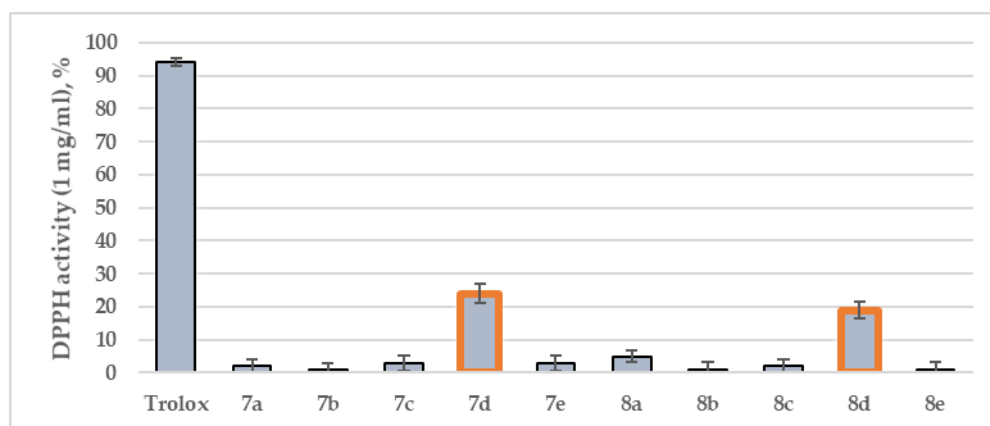


Figure 3. DPPH radical capacities of the newly synthesized compounds **7a–e** and **8a–e** at concentrations of 1 mg/mL. Trolox is used as an internal standard. Data are presented as means from three independent experiments. Standard deviation (SD) (n = 3).

The highest DPPH scavenging activity was achieved by compound **7d** (24%). The β -alanine hydrazide–hydrazone condensed with the same aldehyde (**8d**) demonstrated similar radical scavenging activity (19%). The standard, Trolox, showed 94% DPPH activity. The rest of the newly synthesized molecules demonstrated weak to no antioxidant effects.

2.2.2. ABTS Radical Scavenging Assay

During the 2,2'-azino-bis(3-ethylbenzothiazoline-6-sulphonic acid) (ABTS) assay, the discoloration of the initial color could be detected at 734 nm. The ABTS antioxidant assay of the title compounds is provided in Figure 4.

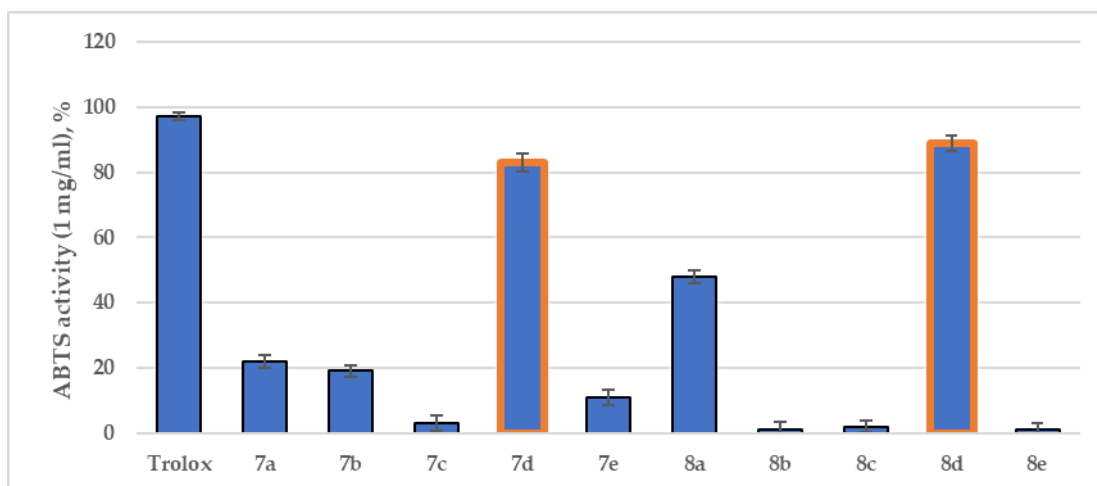


Figure 4. ABTS test of the newly synthesized compounds **7a–e** and **8a–e** at concentrations of 1 mg/mL. Trolox is used as an internal standard. Data are presented as means from three independent experiments. Standard deviation (SD) (n = 3).

2.3. DFT Calculations

To rationalize the antioxidant assays and to determine the favored mechanism involved in free radical scavenging, density functional theory (DFT) calculations were carried out at the B3LYP/6-311++(d,p) level of theory.

2.3.1. Optimized Geometries

The most prominent newly synthesized hydrazide–hydrazones (**7d** and **8d**) were selected for full optimization calculations. An initial conformational search has been

performed by setting 2500 iterations with the OPLS4 force field. The best solutions were further optimized by full DFT geometry optimization at B3LYP/6-311++ (d,p) level of theory. The final geometries of **7d** and **8d** are visualized in Figure 5.

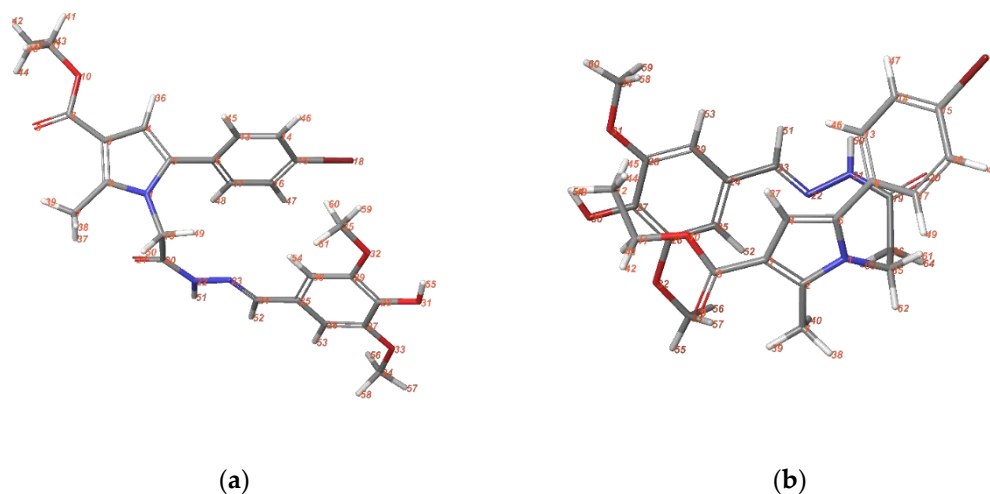


Figure 5. Final optimized geometries of the structures with 2500 iterations with OPLS4 force field. The best solutions for (a) **7d**; (b) **8d** are further optimized at B3LYP/6-311++(d,p).

The overall minimized energies of **7d** and **8d** are -4197 and -4157 Hartree, respectively. It is important to note that *p*-bromophenyl moiety in structure **7d** was located in close proximity to the 3,5-dimethoxy-4-hydroxyphenyl fragment, while the same groups in **8d** were in different positions. In the latter case, the *p*-bromophenyl moiety faced away from the stable conformation. The most stable geometries have been selected as input geometries for further DFT studies.

2.3.2. Analysis of Frontier Molecular Orbitals FMOs and Global Reactivity Descriptors

A quantitative conceptual DFT analysis of the stability and reactivity of the investigated molecules (**7d** and **8d**) was carried out by calculations of the highest occupied molecular orbital (HOMO), the lowest unoccupied molecular orbital (LUMO), and subsequently, the global reactivity descriptors, such as ionization potential (IP), electron affinity (EA), molecular hardness and softness, electronegativity, and electrophilicity. The HOMO-LUMO electronic densities of **7d** and **8d** obtained from the optimized structures with DFT/B3LYP/6-311++(d,p) calculations are given in Figure 6. The blue color was used for a positive phase, and red was used for a negative phase.

It was found that the HOMO of both ligands is localized majorly on the pyrrole ring in **7d** and **8d**, while the LUMO is centered around the hydrazide–hydrazone moiety and the 3,5-dimethoxy-4-hydroxyphenyl fragment. The more energetically favorable conformation of **8d** (-4157 Hartree) led to a more compact structure and, therefore, the localization of HOMO is further spread to the hydrazide–hydrazone and the 3,5-dimethoxy-4-hydroxyphenyl moieties.

The energies (in atomic units) of the FMOs and the global reactivity descriptors (hardness (η), softness (S), electronegativity (χ), chemical potential (μ), and electrophilicity index (ω)) were calculated by applying the Koopman's theorem for closed-shell compounds [16]. The data is reported in Table 3.

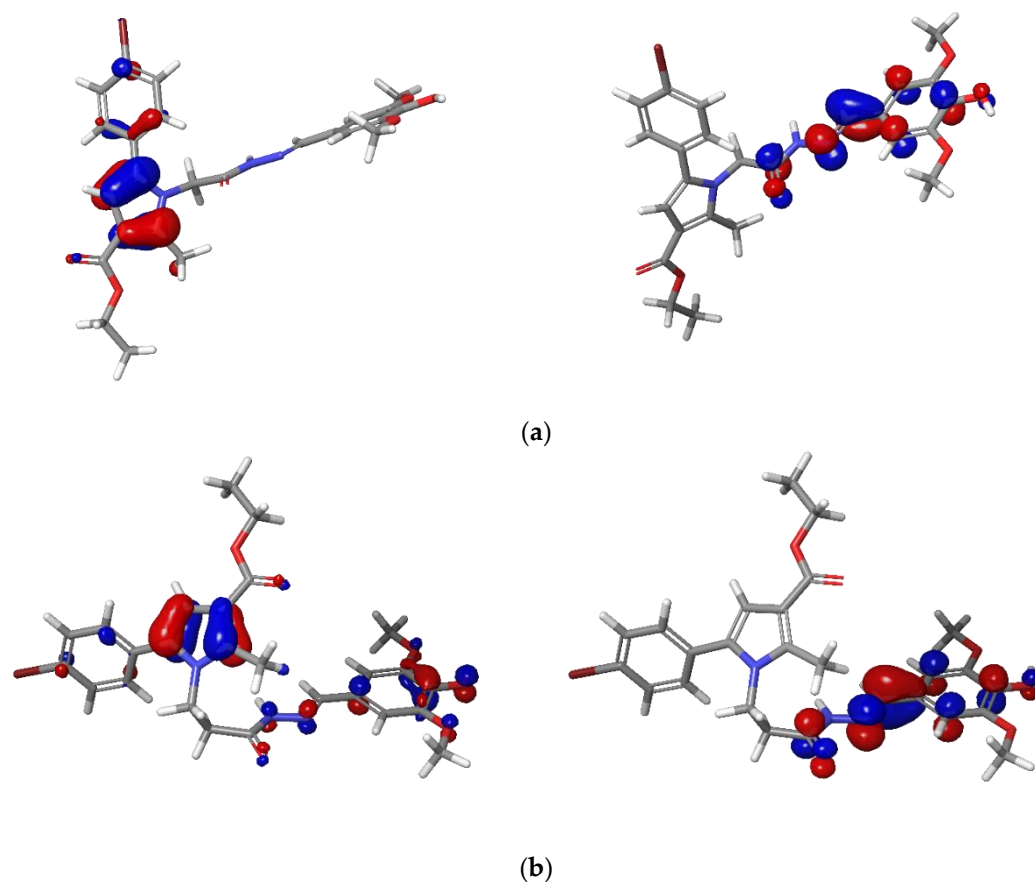


Figure 6. FMOs of **7d** and **8d**, calculated at DFT/B3LYP/6-311++(d,p): (a) HOMO and LUMO of **7d**; (b) HOMO and LUMO of **8d**. The HOMO-LUMO electronic densities are obtained from the optimized structures with DFT/B3LYP/6-311++(d,p) calculations. Blue color indicates a positive phase, and red indicates a negative phase.

Table 3. FMOs energies and global reactivity descriptors for **7d** and **8d** at B3LYP/6-311++(d,p) level of theory.

Electronic Parameter	7d	8d
E_{HOMO}	−0.2013	−0.1976
E_{LUMO}	−0.0564	−0.0470
$\Delta E_{\text{HOMO-LUMO}}$	0.1449	0.1506
Ionization Energy (IP)	0.2013	0.1976
Electron Affinity	0.0564	0.0470
Chemical Hardness	0.0724	0.0753
Softness	6.9060	6.6401
Electronegativity	0.1288	0.1223
Chemical Potential	−0.1288	−0.1223
Electrophilicity Index	0.1145	0.0992

2.3.3. Descriptors of the Antioxidant Properties

The calculated values for the dissociation of hydrogen-connected bonds and the IPs are provided in Table 4.

Table 4. Calculated bond dissociation energies (BDEs) and ionization potentials (IPs) of the corresponding compounds in gas phase.

Compound	Bond	BDE (Kcal/mol)	IP (Kcal/mol)
7d	O ₃₁ -H	83.55	126.31
	C ₇ -H	90.4	
	N ₂₂ -H	95.10	
8d	O ₃₀ -H	83.09	123.99
	C ₇ -H	88.9	
	N ₂₁ -H	96.2	

2.4. In Vitro Evaluations of the Cytotoxicity and Antioxidative Protective Activity on the SH-SY5Y Neuroblastoma Cell Line

2.4.1. Effects of the Newly Synthesized Derivatives 7a–e and 8a–e on the SH-SY5Y Cell Viability

The effects of the newly synthesized N-pyrrolyl-hydrazone derivatives on the cellular viability of neuronal SH-SY5Y cells were evaluated, and the corresponding IC₅₀ values were calculated. In the current study, the cells were seeded at density 2×10^4 and were treated with the test compounds at concentrations 1–500 μM for 24 h. The calculated values of IC₅₀ are presented in Table 5.

Table 5. In vitro cytotoxicity evaluation of the newly synthesized derivatives 7a–e and 8a–e on SH-SY5Y cells (IC₅₀ values).

Compound IDs	IC ₅₀ [μM]	95% Confidence Intervals (CI)
7a	55.75	55.65–61.37
7b	67.60	54.31–79.64
7c	>500	NA
7d	99.56	88.87–103.23
7e	63.08	55.56–73.23
8a	56.33	45.25–67.63
8b	57.36	46.26–68.36
8c	58.23	47.36–69.23
8d	57.26	46.29–68.39
8e	91.07	83.65–105.36
Melatonin	>500	NA

The results demonstrated that compounds 7c, 7d, and 8e possess lackluster or low toxicity on human neuronal SH-SY5Y cells, with IC₅₀ of >500 μM , 99.56 μM , and 91.07 μM , respectively.

2.4.2. Effects of the Newly Synthesized Derivatives 7a–e and 8a–e in a Model of H₂O₂-Induced Oxidative Stress In Vitro

The potential cell protective effects of 7c, 7d, and 8e (the less cytotoxic compounds from the series) were evaluated against H₂O₂-induced oxidative stress in SH-SY5Y cells (Figure 7).

The cells were pre-incubated with the tested compounds at concentrations 1, 10, and 20 μM for 90 min. Melatonin was used as a reference compound because of its well-established neuroprotective effects in various in vitro and in vivo models [17]. After 90 min pre-incubation with the test substances, SH-SY5Y cells were exposed to H₂O₂ (1 mM, 15 min), as described in the Materials and Methods section.

The most potent protection was observed with compound 7c, followed by 7d and 8e. Interestingly, both 7c and 7d showed better protection in all tested concentrations than the reference compound melatonin. It should be noted that compounds 7e and 7d showed statistically significant protection even at the lowest tested concentration (1 μM). Compound 8e showed lower antioxidant protection.

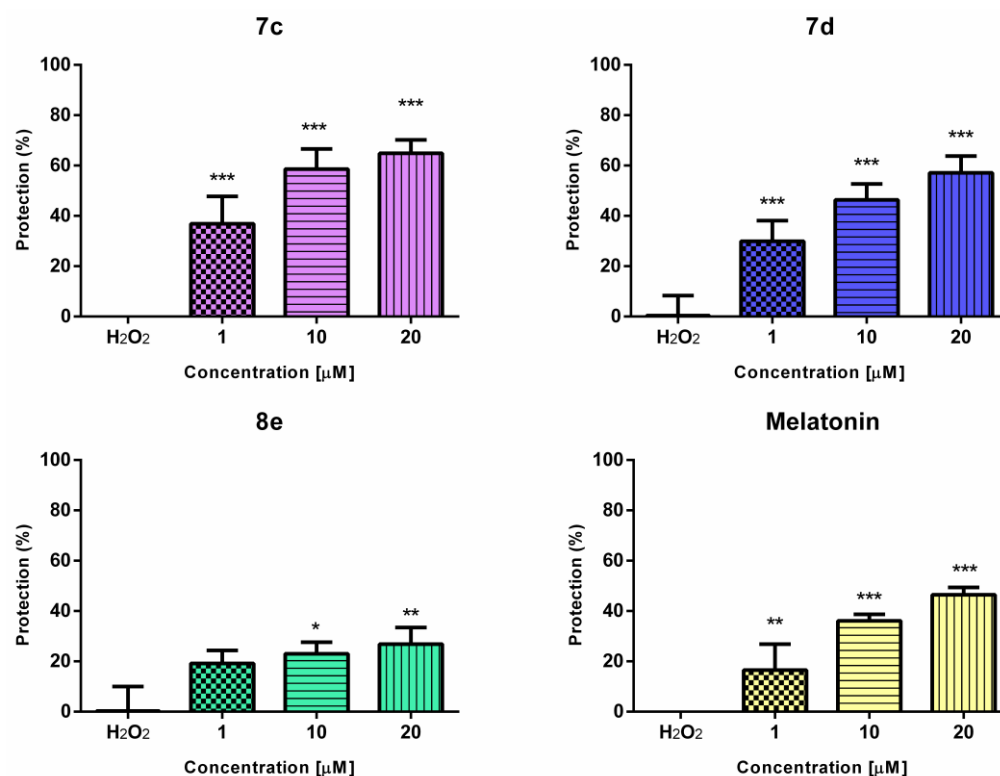


Figure 7. Protective effects of 7c, 7d, 8e, and melatonin in a model of H₂O₂-induced oxidative damage in human neuroblastoma SH-SY5Y cells. Data are presented as means from three independent experiments \pm SD (n = 8). * $p < 0.05$; ** $p < 0.01$; *** $p < 0.001$, vs. H₂O₂ group (one-way analysis of variance with Dunnet's post hoc test).

3. Discussion

3.1. Synthesis

The selection of the applied synthetic path was based on literary data showing the relation between the acidity of the media and the condensation time. Initially, the synthesis was carried out in an ethanol medium without a catalyst, with reaction times of 50–60 min [18]. In an attempt to speed up the process, the same reactions were carried out in an ethanol medium with a catalyst of glacial acetic acid. Under these conditions, the hydrazones were obtained in lower yields of 26–64%, with no significant alteration of the reaction time [19]. Thus, Koopaei presents some data on the interaction of carbohydrazides with carbonyl compounds in an ethanol medium with hydrochloric acid as the catalyst at 100 °C. Applying these conditions, it took 20–30 min to complete the reaction [20,21]. The obtained products were isolated and recrystallized. These conditions did not change either the yield or the time of the condensation.

Thus, in the current work, we conducted the synthesis entirely in glacial acetic acid media. This allowed good yields and optimal time for obtaining pure products (Table 1).

3.2. Antioxidant Assays

Two of the most common assays for the assessment of antioxidant capacities of natural and/or synthetic molecules are the well-applied 2,2'-azino-bis(3-ethylbenzothiazoline-6-sulphonic acid) (ABTS) and 1,1-diphenyl-2-picrylhydrazyl (DPPH) assays. Both techniques are based on spectrophotometric measurement of the quenching of stable colored radicals (ABTS^{•+} or DPPH), which, in turn, allows evaluation of the radical scavenging ability of antioxidants even in complex mixtures [22].

3.2.1. DPPH Radical Scavenging Assay

One of the most common assays for the evaluation of antioxidant effects is the DPPH test. Its frequent applications are mainly due to its relative inexpensiveness [23].

The scavenging activity in the 1,1-diphenyl-2-picrylhydrazyl (DPPH) assay is attributed to the hydrogen-donating ability of antioxidants with a following decrease in the absorbance at 517 nm. The most probable mechanisms of the DPPH-assay are based on hydrogen atom abstraction (HAT) [24], single electron transfer (SET) [25], or mixed mode [26]. The following reaction schemes are related to these mechanisms:



as suggested in [27].

This allowed us to apply this method in order to evaluate the possible radical scavenging effects of the newly synthesized pyrrole-based hydrazones. The obtained results for the target hydrazones are presented in Figure 3.

3.2.2. ABTS Radical Scavenging Assay

In the ABTS^{•+} radical scavenging assay (an electron-transfer-based assay), the 2,2'-azino-bis(3-ethylbenzothiazoline-6-sulfonate) radical cation (ABTS^{•+}), which has a dark blue color, is reduced by an antioxidant into colorless ABTS, which can be measured spectrophotometrically at 734 nm [28].

A literary-based comparative analysis suggested two possible mechanisms of radical scavenging reactions related to the ABTS assay: formation of coupling adducts with ABTS^{•+}—reaction considered as more characteristic for antioxidants of phenolic nature and oxidation without coupling. In addition, the data suggested the possibility for further oxidative degradation of the obtained coupling adducts, leading to hydrazindylidene-like and/or imine-like adducts with 3-ethyl-2-oxo-1,3-benzothiazoline-6-sulfonate and 3-ethyl-2-imino-1,3-benzothiazoline-6-sulfonate as marker compounds, respectively [29].

Considering the presence of a phenyl residue in the structure of the new pyrrole-based hydrazones, it was of interest to compare the possible radical scavenging activity of the target compounds when determined through both the most common in vitro antioxidant assays (Figures 3 and 4). The results from our evaluations demonstrated that when compared to the DPPH test, the ABTS assay revealed significantly better antioxidant capacities for the title compounds. The most prominent antioxidant was **8d**, with 89% scavenging activity, while **7d** showed 83%. Moreover, the hydrazide–hydrazones condensed with 4-dimethylamino benzaldehyde and **7a** and **8a** demonstrated moderate ABTS scavenging capacities of 22% and 48%, respectively. The drastic differences between the two assays could be related to the ability of the ABTS test to examine both hydrophobic and hydrophilic compounds, as well as to test bulky structures [30]. However, the application of the DPPH assay is still used by numerous research groups to produce significant and comparable antioxidant results [31].

In general, the best radical scavenging effect of compounds **7d** and **8d** is quite expected due to the presence of a free *p*-hydroxyl group in the phenyl part of the structure. The appearance of weak radical scavenging properties in the ABTS assay for compounds **7a** and **8a** is probably due to the free electron pair in the N-atom at the *p*-dimethylamino fragment of the phenyl residue. In addition, a negligible effect is observed for **7b**, containing an electron-withdrawing halogen Cl. The presence of *o*-methoxy groups in the phenyl residue is related to the lack of radical scavenging effects in **7e** and **8e**, probably due to the less likely possibility of these groups creating intermolecular hydrogen bonds.

It should also be mentioned that, in general, the shorter series **7a–e** is related to better radical scavenging activity in comparison to the one methylene longer series **8a–e**. This may be due to additional conformational changes leading to the hindrance of the possibility of hydrogen atom transfer and/or electron transfer ability of the active functional groups.

3.3. DFT Calculations

Several mechanisms for free-radical scavenging action of phenyl-containing molecules are proposed, where it is reported that phenolic O–H bond dissociation enthalpy (BDE), adiabatic ionization potential (IP), proton dissociation enthalpy (PDE), proton affinity (PA), and electron-transfer enthalpy (ETE) are important factors used to evaluate the preferred free-radical scavenging pathways of such structures thermodynamically [32]. In an attempt to clarify these mechanisms, some theoretical approaches are applied, with density functional theory (DFT) being most helpful in the calculation of these physicochemical descriptors [33].

The energies of the frontier molecular orbitals and the global reactivity descriptors were calculated with the B3LYP hybrid functional considering recent findings [32]. The corresponding HOMO and LUMO values provide information about the energy distribution and the energetic behavior of the **7d** and **8d**. The comparatively high negative value of HOMO emphasizes the high ability of both compounds to donate electrons to empty molecular orbital energy. Moreover, the negative magnitude of E_{HOMO} and E_{LUMO} establishes the stability of the compounds [34]. The energy gap of the FMOs ($E_{\text{HOMO}}-E_{\text{LUMO}}$) corresponds to the chemical reactivity and the kinetic stability. The calculated frontier molecular energy gaps are 0.1449 a.u and 0.1506 a.u for **7d** and **8d**, respectively. The large gap accounts for hard, unreactive, and less polarizable molecules.

The value of chemical softness (S) and hardness (η) identifies whether the compounds are reactive and can donate electrons. These descriptors are directly correlated with molecular stability and chemical reactivity. When compared, **7d** possesses slightly lower chemical hardness, which corresponds to lower stability. The calculated value of softness revealed that **8d** is more favorable in the charge–transfer mechanism. The negative value of the chemical potential of both ligands (-0.1288 and -0.1223) establishes good stabilities and resistance to sudden decomposition into their elements. The calculated electrophilicity index values (0.1145 and 0.0992 Ha), which are related to chemical potential and hardness, are indicative of the nucleophilicity power [35].

The DFT studies have indicated that the best radical scavenging ligands (**7d** and **8d**) in the newly synthesized molecules are stable, which do not decompose into elements, are less polarizable, and with hard nature. The energy of HOMO revealed that both compounds possess good electron donation capacities.

To examine the most probable mechanism of antioxidant activity of **7d** and **8d**, two processes were observed: hydrogen atom transfer (HAT) and single electron transfer (SET).

The bond dissociation energies (BDE) characterize the viability of hydrogen donation to the free radical. It is considered one of the most important descriptors in the process of determining the antioxidant effects [36]. Thus, the BDE was used as the best reliable thermodynamic parameter describing the hydrogen atom transfer (HAT) mechanism. Because this route involves the H atom transferring from a hydroxyl group of an antioxidant compound to the free radical, the weakest O–H bond with the lowest BDE is expected to be abstracted easier, revealing its higher antiradical (antioxidant) activity. Therefore, a computational calculation of the BDEs of available –OH groups in **7d** and **8d** will benefit in characterizing the theoretical antioxidant mechanism of the compounds. The activity of the –OH groups in both active ligands and the formation of stable radicals was conducted by calculating the dissociation energies.

In addition, apart from the HAT mechanism, another possible pathway for antioxidant molecules is single electron transfer followed by proton transfer (SET-PT). In this route, an electron is transferred from the antioxidant to the free radical, leading to radical cation formation, which subsequently deprotonates. Hence, adiabatic ionization potential (IP) and PDE are the most important parameters in describing the feasibility of the mechanism. In general, lower IPs are more subject to ionization and easier in electron-transfer rate between free radicals and antioxidants [33]. SET is related to the conceptual DFT parameters, mainly the IP energies [37]. This order reveals that compounds **7d** and **8d** are the most active

antioxidants, with all the other calculated IPs being larger than the reference compound Trolox, suggesting their lower activity than Trolox.

The computationally calculated BDEs values of all possible dissociation sites in **7d** and **8d** revealed that radical formation occurs at O₃₁, followed by C₇ and N₂₁. A formation of possible intramolecular stabilization forces could conclude the result of strong N-H bond dissociation in the hydrazide moiety. The O–H bond is the weakest one in both **7d** and **8d**, which describes the potential HAT mechanism in the exerted antioxidant activity. The IPs energies are responsible for the electron donation abilities of the title ligands. The former values of both compounds were higher when compared to the BDEs. Moreover, the relatively low IP energies of the pyrrole-based ligands [38] imply the substantial contribution of the SET mechanism in the antioxidant capacities. Overall, the DFT calculations demonstrated that **7d** and **8d** possess similar values of BDEs and IPs, which provides a good theoretical explanation for the experimental, radical scavenging assays.

3.4. In Vitro Cytotoxicity and Antioxidative Protective Activity on SH-SY5Y Cells

3.4.1. Effects of the Newly Synthesized Derivatives **7a–e** and **8a–e** on SH-SY5Y Cell Viability

Toxicity evaluation of newly synthesized substances in different in vitro models is an important issue in the drug development process.

In the current study, we selected the human neuroblastoma cell line SH-SY5Y as an appropriate model for in vitro neurotoxicity evaluation due to its frequent use in experimental neuroscience [39]. This cell line is also an appropriate model for mimicking various neurodegenerative disorders since its cells are able to convert to numerous types of functional neurons by the introduction of specific compounds. In addition, the SH-SY5Y cells possess tyrosine hydroxylase and dopamine- β -hydroxylase activities because of their sympathetic adrenergic ganglia origin [39], thus making it appropriate for evaluation of dopamine and serotonin modulations in neurodegeneration.

We aimed to evaluate the effects of the newly synthesized N-pyrrolyl hydrazone derivatives **7a–e** and **8a–e** on the cellular viability of the neuronal SH-SY5Y cells and calculated the corresponding IC₅₀ values (Table 5). The results indicated three compounds with low toxicity; among them, compound **7c** may be considered non-toxic with effects comparable to the ones of melatonin. Interestingly, the results showed that the prolongation of the methylene bridge between the central pyrrole ring and the azomethine fragment of the structure with one carbon atom is related to a slight increase in cellular toxicity. The obtained IC₅₀ values showed that the overall cytotoxicity of compounds from series **8a–e** is slightly higher compared to series **7a–e**. Particularly, the toxicity of derivative **8d** is 1.7 times higher than the one of its monomethyl analogue **7d**. Based on their promising safety profile, the compounds **7c**, **7d**, and **8e** were chosen for the further antioxidative protection assay in vitro.

3.4.2. Effects of the Newly Synthesized Derivatives **7a–e** and **8a–e** in a Model of H₂O₂-Induced Oxidative Stress In Vitro

Oxidative stress plays a key role in the damage to the central nervous system and in the pathogenesis of neurodegenerative diseases [40]. When an imbalance between the production of free radicals and detoxification occurs, the high production of ROS can overcome the body's antioxidant defenses, leading to harmful conditions such as oxidative stress and damage to cellular structures and functions.

In addition, free radical overproduction is often considered to be involved in the acute damage of the central nervous system and is strictly related to the development of neurodegenerative diseases. There are a number of facts that determine the free radical overproduction as a direct cause of immature cultured cortical neurons apoptosis [41], induction of DNA damage [42], and necrotic cell death [43], among others [44].

H₂O₂ is one of the most important ROS generated through oxidative stress. It causes oxidative damage in different cell structures such as nucleic acids, proteins, and membrane lipids; therefore, it is commonly used as an in vitro model for inducing oxidative cell

damage [45]. The main mechanism of induction of oxidative stress relates to the production of reactive hydroxyl radicals and the formation of Fenton's reaction, which interacts directly with proteins, lipids, and DNA.

The less cytotoxic compounds **7c**, **7d**, and **8e** were tested for antioxidant protection on the H₂O₂-induced oxidative stress model in neuroblastoma SH-SY5Y cells. As expected, H₂O₂-treatment (1 mM, 15 min) induced a significant decrease in SH-SY5Y cell viability. Our results demonstrated that the pre-treatment with compounds **7c**, **7d**, and **8e** significantly increased the SH-SY5Y cell survival compared to H₂O₂ treatment. Both melatonin and all three test compounds show dose-dependent protective effects. Compared to the reference compound melatonin, at all the applied concentrations between 1 and 20 µM, compounds **7c** and **7d** both exert stronger protective effects, and **8e**'s effect is lower than melatonin's. Noteworthy, despite the stronger radical scavenging activity of **7d** compared to **7c**, shown by both the DPPH and ABTS assay, both compounds cause similar in vitro protective effects on peroxide-damaged SH-SY5Y cells, which may indicate that in the cells, the compounds have pleiotropic modes of antioxidant action.

The overall results from the performed in vitro assessment of the radical scavenging activity and antioxidative protective effects on neuronal SH-SY5Y cells of the newly synthesized N-pyrrolyl hydrazones determined the ethyl 5-(4-bromophenyl)-1-(2-(2-(4-hydroxy-3,5-dimethoxybenzylidene)hydrazine-yl)-2-oxoethyl)-2-methyl-1H-pyrrole-3-carboxylate (**7d**) as the most perspective structure with lowest cytotoxicity, highest radical scavenging activity and best antioxidative protection on H₂O₂-induced oxidative stress model.

3.5. Limitations and Implications Section

Some limitations of the applied assays are related to the specificity of the radical scavenging evaluations used, such as the fact that DPPH and ABTS are not physiological radicals; thus, they are not similar to peroxy-radicals or other oxygen-based radicals. This makes the test an indirect method based on the reduction of persistent radicals. Thus, some discrepancies may be observed since light, oxygen, and pH have an influence on the final absorbance. In this relation, we plan to add some additional cellular evaluations on the effect of the newly obtained substances on cell-defined oxidative mechanisms, which will add to the performed cell protective experiments on H₂O₂-induced oxidative stress applied here. These evaluations include 6-hydroxydopamine (6-OHDA)-, tert-butyl hydroperoxide (tBuOOH)-, and Fe²⁺ ascorbate-induced oxidative stress assays on cellular and sub-cellular levels, which will be published in a following study.

4. Materials and Methods

4.1. Materials

The purity of the obtained compounds and the progress of the reactions were controlled by thin layer chromatography (TLC) on TLC-CardsSilicagel 60 F254, 1.05554, Merck, Darmstadt, Germany, using CHCl₃/CH₃CH₂OH as a mobile phase. Melting points were determined in open capillary tubes on an IA 9200 ELECTROTHERMAL apparatus, Southend-on-Sea, England. All chemical names are given according to IUPAC by the program ChemBioDraw Ultra software, Version 11.0, CambridgeSoft. The IR spectra were performed in the range 400–4000 cm⁻¹ on a Nicoletis10 FT-IR spectrophotometer, using ATR technique with Smart iTR adapter. ¹H-NMR spectra were recorded on a Bruker-Spectrospin WM250 MHz, Faelanden, Switzerland, operating at 250 MHz, as δ (ppm) relative to TMS as internal standard. Mass spectra were registered on a 6410 Agilent LCMS triple quadrupole mass spectrometer (LCMS) with an electrospray ionization (ESI) interface. Elemental analyses were performed on a Euro EA 3000-Single, EUROVECTOR SpA analyser. All chemicals and reagents used as starting materials were purchased from Merck (Darmstadt, Germany).

The necessary for the pharmacological evaluations RPMI cell culture medium, heat-inactivated fetal bovine serum (FBS), L-glutamine, (3-(4,5-dimethylthiazol-2-yl)-2,5-diphenyl-tetrazolium bromide (MTT), hydrogen peroxide (H₂O₂), and dimethyl sulfoxide (DMSO) were acquired from Sigma-Aldrich (Merck KGaA, Darmstadt, Germany).

4.2. General Synthesis of the New Compounds

The corresponding N-pyrrolyl-carbohydrazide **7** or **8** and any of the carbonyl compounds **a**, **b**, **c**, **d**, or **e** (Figure 2) were incubated in a glacial acetic acid in a round bottom flask of 50 mL and stirred at 100 °C to complete the reaction under TLC-control. The obtained products were isolated, washed with diethyl ether, and recrystallized, where necessary, by ethanol.

4.2.1. (E)-ethyl 5-(4-bromophenyl)-1-(2-(2-(4-(dimethylamino)benzylidene)hydrazinyl)-2-oxoethyl)-2-methyl-1H-pyrrole-3-carboxylate (**7a**)

Yield: 84% as an orange powder; m.p. 211.4–213.6; IR (cm⁻¹): 3245 (NH), 2976 (CH₃ and CH₂), 1701 (COOC₂H₅), 1666 (Amide I), 1533 (Amide II), 1232 (C-O), 1073 (C-N), 810 (*p*-substituted C₆H₄), 552 (C-Br); ¹HNMR (δH, 250 MHz, CDCl₃): 1.99 [s, 3H, CH₂CH₃], 2.54 [s, 3H, CH₃(2)], 3.12–3.15 [m, 6H, N(CH₃)₂], 4.20–4.24 [m, 2H, CH₂CH₃], 4.82 [s, 2H, CH₂CO], 6.53 [s, 1H, H(4)], 7.19 [s, 2H, H(3''), H(5'')], 7.21 [s, 2H, H(2''), H(6'')], 7.68–7.69 [d, 2H, H(3'), H(5')], 7.88–7.90 [d, 2H, H(2'), H(6')], 9.99 [s, 2H, NH-N=CH]; LC-MS (ESI): Calc. for C₂₅H₂₈O₃N₄Br [M+H]⁺: 511.1339; Found: 511.1339.; Anal. Calc. for C₂₅H₂₇BrN₄O₃: C, 58.71; H, 5.32. Found: C, 58.68; H, 5.34.

4.2.2. (E)-ethyl 5-(4-bromophenyl)-1-(2-(2-(4-chlorobenzylidene)hydrazinyl)-2-oxoethyl)-2-methyl-1H-pyrrole-3-carboxylate (**7b**)

Yield: 78% as a white powder; m.p. 229.4–231.2; IR (cm⁻¹): 3179 (NH), 2998 (CH₃ and CH₂), 1697 (COOC₂H₅), 1667 (Amide I), 1570 (Amide II), 1240 (C-O), 816 (*p*-substituted C₆H₄), 772 (C-Cl), 557 (C-Br); ¹HNMR (δH, 250 MHz, DMSO-d₆): 1.25–1.29 [m, 3H, CH₂CH₃], 2.44–2.48 [m, 3H, CH₃(2)], 4.14–4.23 [m, 2H, CH₂CH₃], 5.10 [s, 2H, CH₂CO], 6.49 [s, 1H, H(4)], 7.23–7.27 [m, 1H, H(3'')], 7.31–7.36 [m, 1H, H(5'')], 7.46–7.47 [d, 1H, H(6')], 7.50–7.51 [d, 1H, H(2')], 7.58 [s, 1H, H(2'')], 7.59 [s, 1H, H(6'')], 7.68 [s, 1H, H(3')], 7.71 [s, 1H, H(5')], 8.0 [s, 1H, CH=N], 11.81 [s, 1H, CONH]; LC-MS (ESI): Calc. for C₂₃H₂₂O₃N₃BrCl [M+H]⁺: 502.0527; Found: 502.0528.; Anal. Calc. for C₂₃H₂₁BrClN₃O₃: C, 54.94; H, 4.21. Found: C, 54.84; H, 4.29.

4.2.3. (E)-ethyl 5-(4-bromophenyl)-2-methyl-1-(2-(2-(4-nitrobenzylidene)hydrazinyl)-2-oxoethyl)-1H-pyrrole-3-carboxylate (**7c**)

Yield: 76% as a white powder; m.p. 245.9–247.2; IR (cm⁻¹): 3201 (NH), 3064 (CH₃ and CH₂), 1678 (COOC₂H₅), 1592 (Amide I), 1558 (Amide II), 1348 (NO₂), 1240 (C-O), 1205 (C-N), 814 (*p*-substituted C₆H₄), 556 (C-Br); ¹HNMR (δH, 250 MHz, CDCl₃): 1.35–1.37 [m, 3H, CH₂CH₃], 2.58 [s, 3H, CH₃(2)], 4.92 [s, 2H, CH₂CH₃], 5.05 [s, 2H, CH₂CO], 6.65 [s, 1H, H(4)], 7.58 [s, 1H, H(5')], 7.59 [s, 1H, H(3')], 7.78–7.93 [m, 2H, H(2'), H(6')], 8.28 [s, 1H, H(2'')], 8.30 [s, 1H, H(6'')], 8.40 [s, 1H, H(3'')], 8.41 [s, 1H, H(5'')], 10.18 [s, 2H, NH-N=CH]; LC-MS (ESI): Calc. for C₂₃H₂₂O₅N₄Br [M+H]⁺: 513.0768; Found: 513.0766; Anal. Calc. for C₂₃H₂₁BrN₄O₅: C, 53.81; H, 4.12. Found: C, 53.78; H, 4.10.

4.2.4. (E)-ethyl 5-(4-bromophenyl)-1-(2-(2-(4-hydroxy-3,5-dimethoxybenzylidene)hydrazinyl)-2-oxoethyl)-2-methyl-1H-pyrrole-3-carboxylate (**7d**)

Yield: 68% as a white powder; m.p. 191.9–194.4; IR (cm⁻¹): 3424 (OH), 3208 (NH), 3067 (CH₃ and CH₂), 1694 (COOC₂H₅), 1673 (Amide I), 1570 (Amide II), 1236 (C-O), 814 (*p*-substituted C₆H₄), 554 (C-Br); ¹HNMR (δH, 250 MHz, DMSO-d₆): 1.29 [t, 3H, CH₂CH₃], 2.47 [s, 3H, CH₃(2)], 3.77 [s, 6H, OCH₃(3''), OCH₃(5'')], 4.15–4.21 [m, 2H, CH₂CH₃], 5.05 [s, 1H, OH], 5.09 [s, 2H, CH₂CO], 6.50 [s, 1H, H(4)], 6.93 [s, 1H, H(6'')], 6.98 [s, 1H, H(2'')], 7.28–7.38 [m, 2H, H(3'), H(5')], 7.59–7.63 [m, 2H, H(2'), H(6')], 7.89 [s, 1H, CH=N], 11.67 [s, 1H, CONH]; LC-MS (ESI): Calc. for C₂₅H₂₇O₆N₃Br [M+H]⁺: 544.1078; Found: 544.1078; Anal. Calc. for C₂₅H₂₆BrN₃O₆: C, 55.16; H, 4.81. Found: C, 55.15; H, 4.85.

4.2.5. (E)-ethyl 5-(4-bromophenyl)-1-(2-(2-(2,4-dimethoxybenzylidene)hydrazinyl)-2-oxoethyl)-2-methyl-1H-pyrrole-3-carboxylate (**7e**)

Yield: 72% as a white powder; m.p. 206.0–207.6; IR (cm⁻¹): 3234 (NH), 2984 (CH₃ and CH₂), 1698 (COOC₂H₅), 1668 (Amide I), 1520 (Amide II), 1240 (C-O), 822 (*p*-substituted C₆H₄), 554 (C-Br); ¹HNMR (δH, 250 MHz, CDCl₃): 1.36 [t, 3H, CH₂CH₃], 2.54 [s, 3H, CH₃(2)], 3.93 [s, 3H, OCH₃(2'')], 3.94 [s, 3H, OCH₃(4'')], 4.29–4.31 [m, 2H, CH₂CH₃], 4.92 [s, 2H, CH₂CO], 6.64 [s, 1H, H(4)], 6.47 [s, 1H, H(3'')], 6.48 [s, 1H, H(5'')], 7.27 [s, 1H, H(6'')], 7.56 [s, 1H, H(2')], 7.57 [s, 1H, H(6')], 7.82 [s, 1H, H(3')], 7.85 [s, 1H, H(5')], 10.31 [s, 1H, CH=N], 10.32 [s, 1H, CONH]; LC-MS (ESI): Calc. for C₂₅H₂₇O₅N₃Br [M+H]⁺: 528.1129; Found: 528.1132; Anal. Calc. for C₂₅H₂₆BrN₃O₅: C, 56.83; H, 4.96. Found: C, 56.84; H, 4.98.

4.2.6. (E)-ethyl 5-(4-bromophenyl)-1-(3-(2-(4-(dimethylamino)benzylidene)hydrazinyl)-3-oxopropyl)-2-methyl-1H-pyrrole-3-carboxylate (**8a**)

Yield: 86% as a white powder; m.p. 212.0–213.3; IR (cm⁻¹): 3266 (NH), 2907 (CH₃ and CH₂), 1693 (COOC₂H₅), 1668 (Amide I), 1570 (Amide II), 1265 (C-N), 1249 (C-O), 831 (*p*-substituted C₆H₄), 554 (C-Br); ¹HNMR (δH, 250 MHz, CDCl₃): 1.27 [s, 3H, CH₂CH₃], 2.54 [s, 3H, CH₃(2)], 2.59–2.62 [m, 2H, CH₂CH₂CO], 3.12 [s, 3H, N(CH₃)], 3.14 [s, 3H, N(CH₃)], 4.17–4.19 [m, 2H, CH₂CH₂CO], 4.27–4.28 [m, 2H, CH₂CH₃], 6.49 [s, 1H, H(4)], 7.18–7.19 [m, 2H, H(3''), H(5'')], 7.45–7.49 [m, 2H, H(2''), H(6'')], 7.67–7.69 [d, 2H, H(3'), H(5')], 7.95–7.96 [d, 2H, H(2'), H(6')], 8.60 [s, 1H, CH=N], 9.97 [s, 1H, CONH]; LC-MS (ESI): Calc. for C₂₆H₃₀O₃N₄Br [M+H]⁺: 525.1496; Found: 525.1504; Anal. Calc. for C₂₆H₂₉BrN₄O₃: C, 59.43; H, 5.56. Found: C, 59.23; H, 5.66.

4.2.7. (E)-ethyl 5-(4-bromophenyl)-1-(3-(2-(4-chlorobenzylidene)hydrazinyl)-3-oxopropyl)-2-methyl-1H-pyrrole-3-carboxylate (**8b**)

Yield: 74% as a white powder; m.p. 181.4–184.6; IR (cm⁻¹): 3282 (NH), 2931 (CH₃ and CH₂), 1698 (COOC₂H₅), 1668 (Amide I), 1571 (Amide II), 1252 (C-O), 813 (*p*-substituted C₆H₄), 771 (C-Cl), 560 (C-Br); ¹HNMR (δH, 250 MHz, DMSO-d₆): 1.23–1.27 [m, 3H, CH₂CH₃], 2.61 [s, 3H, CH₃(2)], 2.83 [t, 2H, CH₂CH₂CO], 4.13–4.16 [q, 2H, CH₂CH₂CO], 4.24–4.33 [q, 2H, CH₂CH₃], 6.41 [s, 1H, H(4)], 7.35–7.37 [d, 2H, H(3''), H(5'')], 7.51–7.53 [d, 2H, H(2''), H(6'')], 7.56–7.60 [m, 2H, H(2'), H(6')], 7.61–7.63 [d, 1H, H(3')], 7.69–7.71 [d, 1H, H(5')], 7.86 [s, 1H, CH=N], 11.38 [s, 1H, CONH]; LC-MS (ESI): Calc. for C₂₄H₂₄O₃N₃BrCl [M+H]⁺: 516.0684; Found: 516.0684; Anal. Calc. for C₂₄H₂₃BrClN₃O₃: C, 55.78; H, 4.49. Found: C, 55.76; H, 4.48.

4.2.8. (E)-ethyl 5-(4-bromophenyl)-2-methyl-1-(3-(2-(4-nitrobenzylidene)hydrazinyl)-3-oxopropyl)-1H-pyrrole-3-carboxylate (**8c**)

Yield: 82% as a yellow powder; m.p. 214.4–217.1; IR (cm⁻¹): 3294 (NH), 2929 (CH₃ and CH₂), 1689 (COOC₂H₅), 1658 (Amide I), 1572 (Amide II), 1512 (NO₂), 1340 (C-N), 1249 (C-O), 814 (*p*-substituted C₆H₄), 558 (C-Br); ¹HNMR (δH, 250 MHz, CDCl₃): 1.26–1.29 [m, 3H, CH₂CH₃], 2.55 [s, 3H, CH₃(2)], 2.61 [t, 2H, CH₂CH₂CO], 4.18–4.20 [m, 2H, CH₂CH₂CO], 4.21–4.25 [m, 2H, CH₂CH₃], 6.49 [s, 1H, H(4)], 7.17 [s, 1H, H(3')], 7.18 [s, 1H, H(5')], 7.48 [s, 1H, H(6')], 7.49 [s, 1H, H(2')], 8.00 [s, 1H, H(2'')], 8.02 [s, 1H, H(6'')], 8.34 [s, 2H, H(3''), H(5'')], 10.09 [s, 2H, NH-N=CH]; LC-MS (ESI): Calc. for C₂₄H₂₄O₅N₄Br [M+H]⁺: 527.0925; Found: 527.0927; Anal. Calc. for C₂₄H₂₃BrN₄O₅: C, 54.66; H, 4.40. Found: C, 54.64; H, 4.39.

4.2.9. (E)-ethyl 5-(4-bromophenyl)-1-(3-(2-(4-hydroxy-3,5-dimethoxybenzylidene)hydrazinyl)-3-oxopropyl)-2-methyl-1H-pyrrole-3-carboxylate (**8d**)

Yield: 64% as a white powder; m.p. 196.6–197.6; IR (cm⁻¹): 3422 (OH), 3278 (NH), 2971 (CH₃ and CH₂), 1693 (COOC₂H₅), 1666 (Amide I), 1574 (Amide II), 1250 (C-O), 814 (*p*-substituted C₆H₄), 551 (C-Br); ¹HNMR (δH, 250 MHz, DMSO-d₆): 1.22–1.27 [m, 3H, CH₂CH₃], 2.61 [t, 2H, CH₂CH₂CO], 2.64 [s, 3H, CH₃(2)], 3.78 [s, 6H, OCH₃(3''), OCH₃(5'')], 4.12–4.16 [m, 2H, CH₂CH₂CO], 4.20–4.26 [m, 2H, CH₂CH₃], 6.41 [s, 1H, H(4)], 6.80 [s, 1H,

OH], 7.36–7.38 [m, 2H, H(2''), H(6'')], 7.54–7.56 [m, 2H, H(3'), H(5')], 7.62–7.64 [m, 2H, H(2'), H(6')], 7.78 [s, 1H, CH=N], 11.20 [s, 1H, CONH]; LC-MS (ESI): Calc. for C₂₆H₂₉O₆N₃Br [M+H]⁺: 558.1234; Found: 558.1243; Anal. Calc. for C₂₆H₂₈BrN₃O₆: C, 55.92; H, 5.05. Found: C, 55.98; H, 5.02.

4.2.10. (E)-ethyl 5-(4-bromophenyl)-1-(3-(2-(2,4-dimethoxybenzylidene)hydrazinyl)-3-oxopropyl)-2-methyl-1H-pyrrole-3-carboxylate (8e)

Yield: 74% as a white powder; m.p. 170.0–171.9; IR (cm⁻¹): 3298 (NH), 2968 (CH₃ and CH₂), 1692 (COOC₂H₅), 1673 (Amide I), 1571 (Amide II), 1253 (C-O), 813 (*p*-substituted C₆H₄), 549 (C-Br); ¹HNMR (δH, 250 MHz, CDCl₃): 1.24–1.28 [m, 3H, CH₂CH₃], 2.54 [s, 3H, CH₃(2)], 2.58–2.63 [m, 2H, CH₂CH₂CO], 3.18 [s, 3H, OCH₃(4'')], 3.83 [s, 3H, OCH₃(2'')], 4.18–4.20 [m, 2H, CH₂CH₂CO], 4.21–4.23 [m, 2H, CH₂CH₃], 6.37–6.68 [d, 1H, H(3'')], 6.47–6.48 [m, 1H, H(5'')], 6.49 [s, 1H, H(4)], 7.14 [s, 1H, H(3')], 7.18 [s, 1H, H(5')], 7.48 [s, 1H, H(6')], 7.49 [s, 1H, H(2')], 7.73–7.76 [d, 1H, H(6'')], 8.34 [s, 1H, CH=N], 10.22 [s, 1H, CONH]; LC-MS (ESI): Calc. for C₂₆H₂₉O₅N₃Br [M+H]⁺: 542.1285; Found: 542.1293; Anal. Calc. for C₂₆H₂₈BrN₃O₅: C, 57.57; H, 5.20. Found: C, 57.55; H, 5.22.

4.3. Antioxidant Activity Evaluation

4.3.1. DPPH Radical Scavenging Assay

The scavenging assay of the title compounds against DPPH radical was carried out by the widely employed protocol of Brand-Williams et al. [46]. Briefly, a single concentration of 1 mg/mL for each synthesized compound in methanol was obtained. Subsequent addition of 1 mL of the methanol solution of DPPH (1 mmol/L) was performed. The reaction mixtures were incubated in the dark for 30 min. The absorbance was measured at 517 nm. Three measurements were carried out for each sample; 6-Hydroxy-2,5,7,8-tetramethylchroman-2-carboxylic acid (Trolox) was applied as a standard. The percentage inhibition of the tested samples was calculated by the following Formula (3):

$$\text{DPPH}_{\text{scavenging activity}} = \text{Abs}_{\text{control}} - \text{Abs}_{\text{sample}} / \text{Abs}_{\text{control}} \times 100\% \quad (3)$$

where Abs_{control} is the absorbance of the DPPH radical in methanol, and Abs_{sample} is the absorbance of the DPPH radical solution mixed with the sample.

4.3.2. ABTS Radical Scavenging Assay

The ABTS radical tests were measured according to a modified method of Arnao et al. [47]. The test solutions were dissolved in methanol (1 mg/mL) at ambient temperature. The radical cation of ABTS (ABTS^{•+}) was created by mixing 7 mmol/L solution of ABTS and 2.4 mmol/L solution of potassium persulphate, which were set to react for 14 h in the dark at room temperature. The working solutions consisted of 2 mL of the stock solution diluted in 50 mL of methanol with an absorbance of 0.294 ± 0.05 units at 734 nm. Then, 1 mL of the ABTS working solution was allowed to react with the title compounds for 10 min, with a subsequent absorbance determination. The inhibition percentages were evaluated by applying the same formula as the DPPH assay (4).

$$\text{ABTS}_{\text{scavenging activity}} = \text{Abs}_{\text{control}} - \text{Abs}_{\text{sample}} / \text{Abs}_{\text{control}} \times 100\% \quad (4)$$

where Abs_{control} is the absorbance of the ABTS radical in methanol, and Abs_{sample} is the absorbance of the ABTS radical solution mixed with the sample.

4.4. DFT Theoretical Calculations

All of the theoretical computations were carried out by applying Jaguar [48]. The initial geometries for the DFT calculations were achieved after a conformational search with 2500 iterations and OPLS4 force field. Subsequently, full geometry optimizations of the best conformations of compounds 7d and 8d with Becke's three-parameter hybrid exchange–correlation functional (B3LYP) and 6-311++G (d,p) basis set in the gas phase

were performed. It was found that out of 11 functions and 14 basis sets, the most optimal combination in terms of both accuracy and resource usage for bond dissociation energies calculations is M06-2X/6-311G(d,p) [49]. The frontier molecular orbitals and the global reactivity descriptors were calculated at the same level of theory. The bond dissociation energies were obtained with M06-2X and 6-311G basis set considering a recent report [49].

4.5. *In Vitro* Pharmacological Evaluations

4.5.1. Cell Line

Human neuroblastoma cell line SH-SY5Y was purchased from European Collection of Cell Cultures (ECACC, Salisbury, UK). SH-SY5Y cells were cultivated in an RPMI 1640 medium supplemented with 10% heat-inactivated FBS, 2 mM L-glutamine, and 1% antibiotics (penicillin/streptomycin). The cell line was incubated at 37 °C with 5% of CO₂, and the culture's medium was replaced with a time interval of 2–3 days.

4.5.2. Cell Viability Assay

The SH-SY5Y cells were plated for 24 h at 37 °C on 96-well plates at a density of 2×10^4 cells per well to confluence. After 24 h, the cells were treated with the compounds (1–500 µM). MTT assay was performed to measure the metabolic activity in living cells. The mitochondria succinate dehydrogenase system of living cells metabolized yellow-colored, water-soluble, tetrazolium salt MTT (3-(4,5-dimethylthiazol-2-yl)-2,5-diphenyltetrazolium bromide) to a purple insoluble formazan crystal. The cells were incubated with the test solutions for 24 h, the MTT solution (10 mg/mL in PBS) was then added to each well, and the mixture was incubated at 37 °C for 3 h. Thereafter, the MTT solution was carefully aspirated, and the obtained formazan crystals were dissolved by the addition of 100 µL DMSO. The cell viability was determined by measuring the optical density –570–690 nm in a multiplate reader Synergy 2 (BioTek Instruments, Inc., Highland Park, Winooski, VT, USA) [50].

4.5.3. H₂O₂-Induced Oxidative Stress Model in SH-SY5Y Cells

For the H₂O₂-induced oxidative stress model, SH-SY5Y cells were seeded in 96-well plates at a density of 3.5×10^4 /well in 100 µL for 24 h. Afterwards, the cell medium was aspirated, and the cells were treated with different concentrations of tested compounds (1, 10, 20 µM) for 90 min; then, the SH-SY5Y cells were washed with phosphate-buffered saline (PBS) and were exposed to the oxidative stress (H₂O₂ 1 mM in PBS, 15 min). The contents of all wells were changed with culture medium. After 24 h, the amount of attached viable cells was evaluated by MTT assay. Negative controls (cells without hydrogen peroxide treatment) were considered as 100% protection, and hydrogen-peroxide-treated cells as 0% protection.

4.5.4. Statistical Analysis

Statistical analysis of data has been carried out on GraphPad Prism 6 Software. All experiments were carried out in triplicate, and results were presented as mean ± SD (n = 8). Comparisons between groups have been performed by applying one-way ANOVA with Dunnet's multiple comparisons post-test. We performed statistical analyses on the data with the aim of validating the significance of the observed differences. Differences between groups were considered significant for $p < 0.05$, $p < 0.01$ and $p < 0.001$.

5. Conclusions

Ten new N-pyrrolyl hydrazide–hydrazones were synthesized. The structures of the new compounds were elucidated through appropriate IR, ¹H-NMR, and MS spectral data. The purity of the compounds was proven by the corresponding melting points, TLC characteristics, and elemental analyses.

The DFT studies have indicated that the best radical scavenging ligands (**7d** and **8d**) in the newly synthesized compounds are stable molecules that do not decompose into

elements, are less polarizable, and with hard nature. The energy of HOMO revealed that both compounds possess good electron donation capacities. Overall, **7d** and **8d** can readily scavenge free radicals in the biological system by donation of hydrogen atoms and single electron transfer.

The performed in vitro neurotoxicity and cellular toxicity and cell protection evaluations on human neuroblastoma cell line SH-SY5Y determined **7d** as the most prospective with the lowest toxicity and highest antioxidant protection.

Supplementary Materials: The following supporting information can be downloaded at <https://www.mdpi.com/article/10.3390/ph16091198/s1>.

Author Contributions: D.T. contributed to the synthesis of the new molecules; H.K. contributed to the chemical characterization of the new compounds; E.M. contributed to the DFT simulations and analysis; D.S. contributed to the in vitro neuroprotection evaluation; A.D. contributed to the in vitro neuroprotection evaluation; Y.Y. contributed to the in vitro neurotoxicity evaluation; A.M. contributed to in vitro evaluation of the antioxidant activity; V.T. contributed to in vitro neurotoxicity evaluation; M.K.-B. contributed to the in vitro neurotoxicity and neuroprotection evaluation and composing of the manuscript; A.Z. contributed to the composing of the manuscript and the overall data evaluation; M.G. contributed to the initiation of the scientific idea and composing of the manuscript. All authors have read and agreed to the published version of the manuscript.

Funding: This study was financed by the European Union NextGenerationEU through the National Recovery and Resilience Plan of the Republic of Bulgaria, project No. BG-RRP-2.004-0004-C01.

Institutional Review Board Statement: Not applicable.

Informed Consent Statement: Not applicable.

Data Availability Statement: Data is contained within the article and supplementary material.

Acknowledgments: The authors would like to thank Paraskev Nedjalkov for their support in conducting the LC-MS evaluations for structure elucidation.

Conflicts of Interest: The authors declare no conflict of interest.

References

1. Singh, S.; Singh, R.P. In vitro methods of assay of antioxidants: An overview. *Food Rev. Int.* **2008**, *24*, 392–415. [[CrossRef](#)]
2. Linseman, D.A. Targeting oxidative stress for neuroprotection. *Antioxid. Redox Signal.* **2009**, *11*, 421–424. [[CrossRef](#)] [[PubMed](#)]
3. Cho, K.S.; Shin, M.; Kim, S.; Lee, S.B. Recent advances in studies on the therapeutic potential of dietary carotenoids in neurodegenerative diseases. *Oxid. Med. Cell. Longev.* **2018**, *2018*, 4120458. [[CrossRef](#)] [[PubMed](#)]
4. Thurkauf, A.; Yuan, J.; Chen, N.; Wasley, J.W.; Meade, R.; Woodruff, K.H.; Ross, P.C. 1-Phenyl-3-(aminomethyl) pyrroles as potential antipsychotic agents. Synthesis and dopamine receptor binding. *J. Med. Chem.* **1995**, *38*, 4950–4952. [[CrossRef](#)]
5. de Oliveira, K.N.; Costa, P.; Santin, J.R.; Mazzambani, L.; Bürger, C.; Mora, C.; Nunes, R.J.; de Souza, M.M. Synthesis and antidepressant-like activity evaluation of sulphonamides and sulphonyl-hydrazones. *Bioorg. Med. Chem.* **2011**, *19*, 4295–4306. [[CrossRef](#)]
6. Ragavendran, J.V.; Sriram, D.; Patel, S.K.; Reddy, I.V.; Bharathwajan, N.; Stables, J.; Yogeewari, P. Design and synthesis of anticonvulsants from a combined phthalimide–GABA–anilide and hydrazone pharmacophore. *Eur. J. Med. Chem.* **2007**, *42*, 146–151. [[CrossRef](#)]
7. Zlatanova, H.; Vladimirova, S.; Kandilarov, I.; Kostadinov, I.; Delev, D.; Kostadinova, I.; Bijev, A. Analgesic effect of a newly synthesized N-pyrrolylcarboxylic acid in experimental conditions. *Europ. Neuropsychopharmacol.* **2019**, *29*, S468–S469. [[CrossRef](#)]
8. MacLean, P.D.; Chapman, E.E.; Dobrowolski, S.L.; Thompson, A.; Barclay, L.R.C. Pyrroles as antioxidants: Solvent effects and the nature of the attacking radical on antioxidant activities and mechanisms of pyrroles, dipyrirronones, and bile pigments. *J. Org. Chem.* **2008**, *73*, 6623–6635. [[CrossRef](#)]
9. Bhosale, J.D.; Dabur, R.; Jadhav, G.P.; Bendre, R.S. Facile syntheses and molecular-docking of novel substituted 3,4-dimethyl-1H-pyrrole-2-carboxamide/ carbohydrazone analogues with antimicrobial and antifungal properties. *Molecules* **2018**, *23*, 875. [[CrossRef](#)]
10. Peng, Z.; Wang, G.; Zeng, Q.H.; Li, Y.; Wu, Y.; Liu, H.; Wang, J.J.; Zhao, Y. Synthesis, antioxidant and anti-tyrosinase activity of 1,2,4-triazole hydrazones as antibrowning agents. *Food Chem.* **2021**, *341*, 128265. [[CrossRef](#)]
11. Boulebd, H.; Zine, Y.; Khodja, I.A.; Mermer, A.; Demir, A.; Debache, A. Synthesis and radical scavenging activity of new phenolic hydrazone/hydrazide derivatives: Experimental and theoretical studies. *J. Mol. Struct.* **2022**, *1249*, 131546. [[CrossRef](#)]

12. Khodja, A.; Bensouici, C.; Bouleb, H. Combined experimental and theoretical studies of the structure-antiradical activity relationship of heterocyclic hydrazone compounds. *J. Mol. Struct.* **2020**, *1221*, 128858. [[CrossRef](#)]
13. Tzankova, D.G.; Vladimirova, S.P.; Peikova, L.P.; Georgieva, M.B. Synthesis and preliminary antioxidant activity evaluation of new pyrrole based aryl hydrazones. *Bulg. Chem. Commun.* **2019**, *51*, 179–185.
14. Bijev, A.; Georgieva, M. Pyrrole-based hydrazones synthesized and evaluated in vitro as potential tuberculostatics. *Lett. Drug Des. Discov.* **2010**, *7*, 430–437. [[CrossRef](#)]
15. Georgieva, M.; Bijev, A.; Prodanova, P. Synthesis and comparative study of tuberculostatic activity of pyrrole-based hydrazones related to structural variations. *Pharmacia* **2010**, *52*, 3–14.
16. Tsuneda, T.; Song, J.W.; Suzuki, S.; Hirao, K. On Koopmans' theorem in density functional theory. *J. Chem. Phys.* **2010**, *133*, 174101. [[CrossRef](#)]
17. Zhang, Y.; Chen, D.; Wang, Y.; Wang, X.; Zhang, Z.; Xin, Y. Neuroprotective effects of melatonin-mediated mitophagy through nucleotide-binding oligomerization domain and leucine-rich repeat-containing protein X1 in neonatal hypoxic–ischemic brain damage. *FASEB J.* **2023**, *37*, e22784. [[CrossRef](#)]
18. Joshi, S.D.; Kumar, D.; Dixit, S.R.; Tigadi, N.; More, U.A.; Lherbet, C.; Aminabhavi, T.M.; Yang, K.S. Synthesis, characterization and antitubercular activities of novel pyrrolyl hydrazones and their Cu-complexes. *Eur. J. Med. Chem.* **2016**, *121*, 21–39. [[CrossRef](#)]
19. Manvar, A.; Bavishi, A.; Radadiya, A.; Patel, J.; Vora, V.; Dodia, N.; Rawal, K.; Shah, A. Diversity oriented design of various hydrazides and their in vitro evaluation against Mycobacterium tuberculosis H37Rv strains. *Bioorg. Med. Chem. Lett.* **2011**, *21*, 4728–4731. [[CrossRef](#)]
20. Nassiri, K.M.; Assarzadeh, M.J.; Almasirad, A.; Ghasemi-Niri, S.F.; Amini, M.; Kebriaeezadeh, A.; Nassiri, K.N.; Ghadimi, M.; Tabei, A. Synthesis and analgesic activity of novel hydrazide and hydrazine derivatives. *Iran. J. Pharm. Res.* **2013**, *12*, 721–727.
21. Rawat, P.; Singh, R.N. Synthesis, spectral and chemical reactivity analysis of 2,4-dinitrophenyl hydrazone having pyrrole moiety. *J. Mol. Struct.* **2015**, *1097*, 214–225. [[CrossRef](#)]
22. Sujarwo, W.; Keim, A.P. *Spondias pinnata* (L. f.) Kurz. (Anacardiaceae): Profiles and Applications to Diabetes. In *Bioactive Food as Dietary Interventions for Diabetes*, 2nd ed.; Elsevier Inc.: Amsterdam, The Netherlands, 2019; ISBN 978-0-12-813822-9. [[CrossRef](#)]
23. Kedare, S.B.; Singh, R.P. Genesis and development of DPPH method of antioxidant assay. *J. Food Sci. Technol.* **2011**, *48*, 412–422. [[CrossRef](#)] [[PubMed](#)]
24. Dawidowicz, A.L.; Olszowy, M.; Józwick-Doleba, M. Importance of solvent association in the estimation of antioxidant properties of phenolic compounds by DPPH method. *J. Food Sci. Technol.* **2015**, *52*, 4523–4529. [[CrossRef](#)]
25. Brizzolari, A.; Foti, M.C.; Saso, L.; Ciuffreda, P.; Lazarević, J.; Santaniello, E. Evaluation of the radical scavenging activity of some representative isoprenoid and aromatic cytokinin ribosides (N6-substituted adenosines) by in vitro chemical assays. *Nat. Prod. Res.* **2022**, *36*, 6443–6447. [[CrossRef](#)]
26. Schaich, K.M. Lipid oxidation in specialty oils. In *Nutraceutical and Specialty Oils*; Shahidi, F., Ed.; CRC Press/Taylor & Francis: London, UK, 2006; pp. 401–448.
27. Amarowicz, R.; Pegg, R.B. Functional Food Ingredients from Plants. In *Advances in Food and Nutrition Research*; Elsevier Inc.: Amsterdam, The Netherlands, 2019.
28. Dasgupta, A.; Klein, K. Methods for Measuring Oxidative Stress in the Laboratory. In *Antioxidants in Food, Vitamins and Supplements*; Elsevier Inc.: Amsterdam, The Netherlands, 2014. [[CrossRef](#)]
29. Ilyasov, I.R.; Beloborodov, V.L.; Selivanova, I.A.; Terekhov, R.P. ABTS/PP Decolorization assay of antioxidant capacity reaction pathways. *Int. J. Mol. Sci.* **2020**, *21*, 1131. [[CrossRef](#)]
30. Mateev, E.; Georgieva, M.; Zlatkov, A. Design, microwave-assisted synthesis, biological evaluation, molecular docking, and adme studies of pyrrole-based hydrazide-hydrazones as potential antioxidant agents. *Maced. J. Chem. Chem. Eng.* **2022**, *41*, 175–186. [[CrossRef](#)]
31. Munteanu, I.G.; Apetrei, C. Analytical methods used in determining antioxidant activity: A Review. *Int. J. Mol. Sci.* **2021**, *22*, 3380. [[CrossRef](#)] [[PubMed](#)]
32. Leopoldini, M.; Russo, N.; Toscano, M. The molecular basis of working mechanism of natural polyphenolic antioxidants. *Food Chem.* **2011**, *125*, 288–306. [[CrossRef](#)]
33. Farrokhnia, M. Density Functional Theory Studies on the Antioxidant Mechanism and Electronic Properties of Some Bioactive Marine Meroterpenoids: Sargahydroquionic Acid and Sargachromanol. *ACS Omega* **2020**, *5*, 20382–20390. [[CrossRef](#)]
34. Safna Hussan, K.P.; Shahin Thayyil, M.; Rajan, V.K.; Muraleedharan, K. DFT studies on global parameters, antioxidant mechanism and molecular docking of amlodipine besylate. *Comput. Biol. Chem.* **2019**, *80*, 46–53. [[CrossRef](#)]
35. Choudhary, V.K.; Bhatt, A.K.; Dash, D.; Sharma, N. DFT calculations on molecular structures, HOMO–LUMO study, reactivity descriptors and spectral analyses of newly synthesized diorganotin (IV) 2-chloridophenylacetohydroxamate complexes. *J. Comput. Chem.* **2019**, *40*, 2354–2363. [[CrossRef](#)] [[PubMed](#)]
36. Dávalos, J.Z.; Valderrama-Negrón, A.C.; Barrios, J.R.; Freitas, V.L.S.; Ribeiro da Silva, M.D.M.C. Energetic and structural properties of two phenolic antioxidants: Tyrosol and hydroxytyrosol. *J. Phys. Chem. A* **2018**, *122*, 4130–4137. [[CrossRef](#)] [[PubMed](#)]
37. Liang, N.; Kitts, D.D. Antioxidant property of coffee components: Assessment of methods that define mechanisms of action. *Molecules* **2014**, *19*, 19180–19208. [[CrossRef](#)]
38. Lu, L.; Qiang, M.; Li, F.; Zhang, H.; Zhang, S. Theoretical investigation on the antioxidative activity of anthocyanidins: A DFT/B3LYP study. *Dyes Pigment.* **2014**, *103*, 175–182. [[CrossRef](#)]

39. Lopez-Suarez, L.; Al Awabdh, S.; Coumoul, X.; Chauvet, C. The SH-SY5Y human neuroblastoma cell line, a relevant in vitro cell model for investigating neurotoxicology in human: Focus on organic pollutants. *Neurotoxicology* **2022**, *92*, 131–155. [[CrossRef](#)]
40. Wang, X.; Zhou, Y.; Gao, Q.; Ping, D.; Wang, Y.; Wu, W.; Lin, X.; Fang, Y.; Zhang, J.; Shao, A. The Role of exosomal microRNAs and oxidative stress in neurodegenerative diseases. *Oxid. Med. Cell. Longev.* **2020**, *2020*, 3232869. [[CrossRef](#)]
41. Ratan, R.R.; Murphy, T.H.; Baraban, J.M. Oxidative stress induces apoptosis in embryonic cortical neurons. *J. Neurochem.* **1994**, *62*, 376–379. [[CrossRef](#)]
42. Floyd, R.A.; Carney, J.M. Free radical damage to protein and DNA: Mechanisms involved and relevant observations on brain undergoing oxidative stress. *Ann. Neurol.* **1992**, *32* (Suppl. S1), S22–S27. [[CrossRef](#)]
43. Kane, D.J.; Sarafian, T.A.; Anton, R.; Hahn, H.; Gralla, E.B.; Valentine, J.S.; Ord, T.; Bredesen, D.E. Bcl-2 inhibition of neural death: Decreased generation of reactive oxygen species. *Science* **1993**, *262*, 1274–1281. [[CrossRef](#)]
44. Amoroso, S.; Gioielli, A.; Cataldi, M.; Di Renzo, G.; Annunziato, L. In the neuronal cell line SH-SY5Y, oxidative stress-induced free radical overproduction causes cell death without any participation of intracellular Ca²⁺ increase. *Biochim. Biophys. Acta Mol. Cell Res.* **1999**, *1452*, 151–160. [[CrossRef](#)]
45. Salminen, A.; Kaarniranta, K.; Kauppinen, A. Crosstalk between oxidative stress and SIRT1: Impact on the aging process. *Int. J. Mol. Sci.* **2013**, *14*, 3834–3859. [[CrossRef](#)] [[PubMed](#)]
46. Brand-Williams, W.; Cuvelier, M.E.; Berset, C. Use of a free radical method to evaluate antioxidant activity. *LWT Food Sci. Technol.* **1995**, *28*, 25–30. [[CrossRef](#)]
47. Arnao, M.B.; Cano, A.; Hernández-Ruiz, J.; García-Cánovas, F.; Acosta, M. Inhibition by L-ascorbic acid and other antioxidants of the 2,2'-azino-bis(3-ethylbenzthiazoline-6-sulfonic acid) oxidation catalyzed by peroxidase: A new approach for determining total antioxidant status of foods. *Anal. Biochem.* **1996**, *236*, 255–261. [[CrossRef](#)] [[PubMed](#)]
48. Bochevarov, A.D.; Harder, E.; Hughes, T.F.; Greenwood, J.R.; Braden, D.A.; Philipp, D.M.; Rinaldo, D.; Halls, M.D.; Zhang, J.; Friesner, R.A. Jaguar: A high-performance quantum chemistry software program with strengths in life and materials sciences. *Int. J. Quantum Chem.* **2013**, *113*, 2110–2142. [[CrossRef](#)]
49. Spiegel, M.; Gamian, A.; Sroka, Z. A statistically supported antioxidant activity dft benchmark—the effects of hartree-fock exchange and basis set selection on accuracy and resources uptake. *Molecules* **2021**, *26*, 5058. [[CrossRef](#)]
50. Mosmann, T. Rapid colorimetric assay for cellular growth and survival: Application to proliferation and cytotoxicity assays. *J. Immunol. Methods* **1983**, *65*, 55–63. [[CrossRef](#)]

Disclaimer/Publisher's Note: The statements, opinions and data contained in all publications are solely those of the individual author(s) and contributor(s) and not of MDPI and/or the editor(s). MDPI and/or the editor(s) disclaim responsibility for any injury to people or property resulting from any ideas, methods, instructions or products referred to in the content.